



1 **Disentangling the chemistry and transport impacts of the** 2 **Quasi-Biennial Oscillation on stratospheric ozone**

3 Jinbo Xie¹, Qi Tang¹, Michael Prather², Jadwiga Richter³, Shixuan Zhang⁴

4 ¹Lawrence Livermore National Laboratory, Livermore, CA, USA

5 ²Department of Earth System Science, University of California, Irvine, CA, USA

6 ³National Center for Atmospheric Research, Boulder, CO, USA

7 ⁴Pacific Northwest National Laboratory, Richmond, CA, USA

8 Correspondence to: Jinbo Xie (xie7@llnl.gov)

9

10 **Abstract**

11 The quasi-biennial oscillation (QBO) in tropical winds perturbs stratospheric ozone
12 throughout much of the atmosphere via changes in transport of ozone and other trace gases and
13 via temperature changes that alter chemical processes. Here we separate the temperature-driven
14 changes using the Department of Energy's Energy Exascale Earth System Model version 2
15 (E3SMv2) with linearized stratospheric ozone chemistry. E3SM produces a natural QBO cycle
16 in winds, temperature, and ozone. Our analysis defines climatological QBO patterns of ozone for
17 the period 1979-2020 using both nonlinear principal component analysis and monthly
18 composites centered on QBO phase shift. As a climate model, E3SM cannot predict the timing of
19 the phase shift, but it does match these climatological patterns. We develop an offline version of
20 our stratospheric chemistry module to calculate the steady-state response of ozone to temperature
21 and overhead ozone perturbations, assuming that other chemical families involved in ozone
22 chemistry remain fixed. We find a clear demarcation: ozone perturbations in the upper
23 stratosphere (above 20-hPa) are predicted by the steady-state response of the ozone column to
24 the temperature changes; while those in the lower stratosphere show no temperature response
25 and are presumably driven by circulation changes. These results are important for diagnosing
26 model-model differences in the QBO-ozone responses for climate projections.

27



28 **1. Introduction**

29 The Quasi-Biennial Oscillation (QBO) is the principal mode of dynamical variability in the
30 tropical stratosphere, with impact on the circulation and greenhouse gases that extends from the
31 tropical stratosphere into the troposphere. Its effect on ozone – the most important trace gas in
32 the stratosphere – has been well studied (Reed 1964; Bowman, 1989; Wang et al., 2022). Despite
33 being a robust research area for decades, assigning the pattern of ozone perturbations over the
34 QBO cycle to specific processes is not easy due to the simultaneous temperature and transport
35 changes (Plumb and Bell, 1982) and the photochemical linkages across most all reactive gases.

36 This study aims to provide a better understanding of what drives ozone variability over the
37 QBO cycle. We develop a new index of the QBO phase from a nonlinear principal component
38 analysis (NLPCA) of the tropical zonal winds that retains the observed asymmetric pattern and
39 provides a more consistent measure of the phase throughout the cycle, not just when the zonal
40 winds change sign. Second, we create phase-based composite diagrams to investigate the
41 temporal evolution of ozone patterns, both observed and modeled. Our primary modeling tool is
42 the Department of Energy (DOE) Energy Exascale Earth Model version 2 (E3SMv2, Golaz et
43 al., 2022) with interactive stratospheric ozone (Linoz v2, McLinden et al., 2000), and secondarily
44 we examine some QBO experiments from the National Center for Atmospheric Research
45 (NCAR) Community Earth System Model (CESM). We find that QBO cycles in ozone can be
46 attributed to temperature perturbations in the upper stratosphere (above 20-hPa) and mostly to
47 circulation changes in the lower stratosphere over a wide range of latitudes. The observational
48 data and ozone modeling are described in section 2. The NLPCA method is presented in section
49 3, followed by the description and use of the Linoz off-line chemistry model in section 4. The
50 results are in section 5. The discussion and conclusion are in section 6.

51 **2. The QBO**

52 **2.1 Overview**

53 The QBO appears prominently as alternating easterly and westerly equatorial winds that
54 propagate downward from the top (50 km) to the bottom (16 km) of the stratosphere with a
55 period of about 28 months (Baldwin et al., 2001; Anstey and Shepherd, 2014; Coy et al., 2016).
56 Associated with this propagation of the alternating equatorial winds, the QBO also modifies the
57 vertical propagation of planetary waves and creates global changes in the Brewer-Dobson



58 Circulation (BDC) (Holton and Tan, 1982; Watson and Gray, 2014; Zhang et al., 2020). Through
59 perturbations to the BDC, the QBO has been identified as an important source of variability in
60 the overall chemical composition of the tropical stratosphere (Randel et al., 1998; Shuckburgh et
61 al. 2001; Park et al. 2017), and it reaches into the troposphere through stratosphere-troposphere
62 exchange (STE) of ozone (Yang and Tung, 1995; Kinnersley and Tung, 1999) and nitrous oxide
63 (Hamilton, 1989; Ruiz et al., 2021).

64 **2.2 Ozone impacts**

65 The QBO affects ozone through coupled transport and chemical processes, limiting our
66 ability to ascribe the cause of ozone perturbations to specific processes. Baldwin et al. (2001)
67 suggest that the dynamic impact of the QBO via direct transport of ozone accounts for most of
68 the ozone variability. The primary mechanism being: maximum westerly winds correspond to
69 warmer temperatures that result in diabatic cooling that slower tropical ascent of air parcels, with
70 the opposite sense (more rapid ascent) for easterly winds. Tropical ozone has a steep, inverted
71 gradient, 0.1 parts per million (ppm = micromol mol⁻¹) at 100 hPa peaking to 10 ppm at 10 hPa.
72 In this region ozone values are below photochemical steady-state with production exceeding
73 loss, and thus slower ascent rates lead to greater accumulation of ozone, including in total
74 column ozone (TCO, Reed, 1964). This ozone anomaly is also impacted by vertical shifts in
75 NO_y (total reactive nitrogen reservoir), which photochemically destroys ozone (Chipperfield and
76 Gray, 1992; Chipperfield et al., 1994, Politowicz and Hitchman, 1997; Jones et al., 1998). The
77 QBO pattern in ozone reverses phase outside of the core tropics (15°S - 15°N), consistent with
78 the return arm of the local equatorial QBO circulation (Holton et al., 1989; Gray and Dunkerton,
79 1990).

80 **2.3. The QBO modeling initiative**

81 Tropical stratospheric variability, in particular the QBO, has been poorly represented in
82 climate models (Butchart et al., 2011; Butchart et al., 2018; Richter et al., 2020). The number of
83 models with a naturally generated QBO was 0 in the third Coupled Model Intercomparison
84 Project (CMIP3); it rose to 5 in CMIP5 and to 15 in CMIP6 (Richter et al., 2020). Even when
85 models naturally produce a QBO-like variability, the amplitude and periods often fail to match
86 the observed pattern. In the current Chemistry–Climate Model Initiative (CCMI), many of the
87 CCMs forced a QBO signal by nudging the equatorial zonal wind (Morgenstern et al., 2017).
88 Nudging of the winds is inherently unphysical and produces an anomalous BDC not found



89 in the free-running versions of the same CCMs (Orbe et al., 2020). The World Climate Research
90 Project (WCRP) Atmospheric Processes And their Role in Climate (APARC) started an QBO
91 initiative (QBOi) in 2015 to improve CCM simulation of tropical variability (Butchart et al.,
92 2018), and here we build on those experiments.

93 **2.4. CCM models**

94 The primary model for this study is E3SMv2. E3SM's atmospheric component (EAMv2) is
95 run as a CCM with specified sea surface temperatures (SSTs) and has 72 vertical layers and a
96 horizontal resolution of about 100 km. Following Richter et al. (2010), EAMv2 employs gravity
97 wave (GW) parameterizations that include orographic GWs (McFarlane, 1987), convective GWs
98 (Beres et al., 2004), and GWs generated by frontal systems (Charron and Manzini, 2002).
99 Tunable parameters in the orographic and frontal GW parameterizations remain the same as in
100 EAMv1 (Xie et al., 2018; Rasch et al., 2019). The tunable parameters in convective GWs were
101 explored to produce a more realistic QBO in EAMv2 with a period around 27 months, much
102 closer to observations (28 months) as compared to 16 months in EAMv1 (Richter et al., 2019).
103 Nevertheless, the modeled QBO remains very weak in terms of amplitude. Stratospheric ozone
104 in E3SMv2 is calculated interactively through transport and the chemical Linoz module
105 (McLinden et al., 2000; Hsu and Prather, 2009) that was updated from the E3SM O3v1 to O3v2
106 module (Tang et al., 2021). Linoz v2 data tables are used to calculate the 24-hour-average ozone
107 tendency (i.e., net production minus loss) from an adopted climatological mean state for key
108 species (CH_4 , H_2O , and NO_y , Cly, Bry) and first-order Taylor series expansions about the local
109 ozone, temperature, and overhead ozone column (see Eq. (3) in Sect. 5.1). The data tables are
110 generated for each year assuming key chemical species (CH_4 , H_2O , and NO_y , Cly, Bry) follow
111 monthly zonal-mean climatologies that scale with the slowly varying changes in tropospheric
112 mean abundance of their source gases (e.g., N_2O , CFCs, halons, CH_4 , tropopause H_2O). The
113 Linoz model produces a reasonable stratospheric ozone climatology, including seasonal and
114 interannual variability and the Antarctic ozone hole (Tang et al., 2021; Ruiz and Prather, 2022).
115 The tropospheric chemical package for E3SMv2 (chemUCI) was not used and the lower
116 boundary for Linoz was set to 30 ppb. Thus, none of the ozone column variability arises from
117 tropospheric ozone chemistry. E3SMv2 diagnostics on the tendency of tropospheric ozone
118 enable the geographically resolved stratosphere-troposphere exchange (STE) flux of ozone every
119 time step (Hsu et al., 2005; Tang et al., 2013).



120 The secondary model for this study is CESM2 (Emmons et al., 2020), using a modified
121 version of the community atmosphere model (CAM) with 83 vertical levels (Randall et al., 2023;
122 Isla et al., 2024), and also run as a CCM with specified sea surface temperatures (SSTs). CAM
123 uses the finite-volume dynamical core with a nominal 1° horizontal resolution and with physics
124 from the Whole Atmosphere Community Climate Model version 6 (WACCM6; Gettleman et al.
125 2019). The parameters for the convective GW momentum transport were tuned especially for
126 this version to obtain a realistic, naturally generated QBO. The inline ozone calculation is
127 replaced with a monthly mean 3D ozone climatology specified from a previous WACCM
128 simulation. This ozone forcing is formed by merging WACCM simulations for historical (1850-
129 2014) and future period (2015-2100). The ensemble mean of three historical WACCM
130 simulations is used for the historical period while one future scenario run is used for future
131 period. As the mean of free-running CCM simulations, this WACCM ozone climatology does
132 not have any significant QBO-like variability, and thus it cannot trigger a QBO in the CCM
133 (Butchart et al., 2023).

134 With these two different types of simulations, one with interactive ozone and one without, we
135 must limit our analysis with the pair of models to examining the forced dynamical response
136 (temperature, circulation), but will use the E3SM results to compare the modeled QBO-ozone
137 response with observations.

138 **2.5. Observed ozone and wind**

139 For ozone, we derive the observed QBO signal from the monthly zonal mean total column
140 ozone (TCO) using the Multi-Sensor Reanalysis version 2 data (MSRv2, R.J. van der A, et al.
141 2015). This latitude-by-month dataset initially covers the period 1979-2012 and later extended to
142 2020. For stratospheric profiles, we use the zonal monthly mean latitude-by-altitude from the
143 Concentration Monthly Zonal Mean (CMZM) product (Sofieva et al., 2023). This altitude-by-
144 month profile data covers the period 1985-2020. The vertical levels are converted to pressure
145 levels inverting the pressure-altitude formula, $z^* = 16 \log_{10}(1000/P)$ km. We compared this
146 ozone data with the overlapping period from the Microwave Limb Sounder (MLS) data (V5
147 Level 3; Schwartz et al., 2021) and found only small differences with regard to QBO patterns.

148 We use data from the ERA5 reanalysis produced by the European Center for Medium-Range
149 Weather Forecast (ECMWF) Integrated Forecast System (Hersbach et al., 2020). The version we
150 use has 137 hybrid sigma model levels from the surface to the model top at 0.01 hPa, and the



horizontal resolution is about 31 km. We use monthly ERA5 data (wind, temperature, geopotential height) for the period 1979–2020 to analyze the QBO-related dynamical changes, and 6-hourly ERA5 tropical zonal wind (15°N–15°S) to nudge model simulations mentioned below. We use the 5°S–5°N tropical average zonal wind from ERA5 and simulations to determinate the QBO phase index. The combined station zonal wind data from Freie University of Berlin (Naujokat, 1986) for the period of 1979–2020 is also used in the NLPCA analysis (Fig. 1).

2.6 The QBOi simulations

We use a set of three experiments from our two models following the protocol for phase-2 of the QBOi (Butchart et al., 2018; Bushell et al., 2020; Richter et al., 2020):

- (1) Exp1-ObsQBO (nudged): the zonal wind (i.e., u) in the tropical stratosphere is constrained to follow the observed QBO evolution by nudging it toward ERA5 reanalysis (Hitchcock et al. 2022). Thus, the stratospheric climate in the tropics is constrained.
- (2) Exp1-AMIP (natural): the zonal wind in the tropical stratosphere evolves freely in each CCM being forced only by SSTs and trace-gas radiative heating; there is no nudging.

The nudging is applied to the zonal wind over the range 8 hPa-to-80 hPa and 15°S-to-15°N (Supplementary Fig. 1, nudging coefficient shown is for E3SMv2, that for CESM2 is similar). There is a slight difference in how the models were nudged: E3SMv2 is nudged to the 3-D ERA5 wind field, while CESM2 is nudged to a 2-D zonally-averaged ERA5 wind field. The nudging relaxation timescale is 5 days, which is expected to constrain the slowly evolving QBO winds.

3. NLPCA analysis of QBO phase

In diagnosing QBO-related changes to the dynamics and chemistry, we need to define the phases of successive QBOs, at least and align these phases over a 24-month period. Asymmetric and nonlinear features of the evolution of the QBO phase are found in many studies (Lindzen and Holton 1968; Holton and Lindzen, 1972; Giorgetta et al., 2002). The most obvious and sharp synchronization point is when the QBO west phase (QBOW, i.e. prevailing westerlies) transitions to the east phase (QBOe: prevailing easterlies) at some pressure level in the middle stratosphere (taken as 10 hPa here) (Naujokat et al., 1986; Pahlavan et al., 2021; Kang et al., 2022). The QBOe phase is typically longer (e.g., 63%, Bushell et al., 2019), with wind speeds about twice as strong as that of the QBOW (Naujokat et al., 1986; Kang et al., 2022). The problem with defining the QBO phase (index) simply as the absolute time difference relative to the synchronization



182 point (e.g., Ruiz et al., 2021) is that the duration of different phases varies across successive
183 QBOs.

184 Previous use of PCA-derived QBO indices (Hamilton and Hsieh, 2002; Lu et al., 2009) did
185 not allow for this asymmetric and nonlinear behavior. Lu et al. (2009) noted that the
186 reconstructed wind series from the PCA looked more sinusoidal in time than the actual winds,
187 and thus the asymmetries between phases did not show up in the PCA-based indices. To address
188 these issues, we use an NLPCA method that utilizes hierarchical-type neural network with an
189 auto-associative architecture (Scholz et al. 2002). It is a nonlinear generalization of the standard
190 PCA from straight lines to curves in the original data space, and natural extension to the PCA
191 method by enforcing the nonlinear components to the same hierarchical order as in the standard
192 PCA (Scholz et al., 2002). The NLPCA model described here has 5 layers with 3 hidden layers
193 of neurons. The layers of the neural-network for NLPCA are in the sequence of input-encoding-
194 bottleneck-decoding-output with the structure of $n-(2k+2)-k-(2k+2)-n$, where the n refers to
195 dimension of input/output dataset and k is the number of dimensions for bottleneck layer. To
196 achieve robustness, the NLPCA is applied to the tropical zonal wind data (5°S - 5°N , 10-hPa to
197 70-hPa) for a set of k varying from 2 to 5, with 100 runs (different in random initialization
198 weights) for each k . The optimal number of k is set as 5 as it gives the lowest root-mean-square-
199 error between the input and output. It is shown that the first and second principal components
200 (PC1 and PC2) of the NLPCA account for approximately 90% of the whole variance.

201 Following previous studies (Wallace et al., 1993; Hamilton and Hsieh, 2002; Lu et al., 2009),
202 the QBO phase index ψ is calculated using PC1 and PC2 as follows:

203
$$\psi = \arctan(v/u) \quad (-\pi \leq \psi \leq \pi), \quad (1)$$

204 where u and v are the time series of the PC1 and PC2, respectively. The positive/negative phase
205 angle index ψ corresponds to QBOw/QBOe.

206 We compare the reconstructed zonal wind anomalies using NLPCA and PCA (Wallace et
207 al., 1993) with the QBO cycle in the observation (Fig. 1). It is shown that the observed QBO
208 transition corresponds to an abrupt downward propagation in QBOw and a slower downward
209 transition in QBOe (indicated by clustering points in B to C to A on black triangular shape in
210 Fig. 1a). The NLPCA captures large part of this sharp transition in QBOw while PCA
211 underestimates it (indicated by points near C in Fig. 1a). This difference is also clearly shown in
212 a typical QBO cycle of 1970.9 – 1972.3 (Figs. 1b, 1b, and 1d, black arrow-sticks exhibits the



213 downward propagation in QBOw) and the time series of NLPCA/PCA QBO phase (index) (Fig.
214 S2).

215 While the NLPCA-derived QBO index is more realistic in following the atmospheric
216 changes, it is impractical to map the NLPCA phases onto the monthly-mean model diagnostics.
217 Thus, our QBO composites use simple monthly time steps about our best synchronization point,
218 which from the NLPCA analysis we take to be the transition from easterlies to westerlies at when
219 phase angle index ψ crosses 0 with negative values before and positive values after it. It is
220 demonstrated that compared to QBO composites produced using the PCA-derived QBO index,
221 that produced using the NLPCA-derived index show larger contrast in observed tropical zonal
222 wind anomalies between QBOw/QBOe (Supplementary Figs. 3a and 3b) that is consistent with
223 those described in previous literatures (Hamilton and Hsieh, 2002; Lu et al., 2009). This larger
224 contrast between NLPCA and PCA in zonal wind anomalies is correspondent with the larger
225 contrast in that of the total column ozone anomalies (Supplementary Figs. 3c and 3d).

226 **4. Linoz calculation of the steady-state ozone**

227 To examine the ozone response to the QBO we use the Linoz model, and the steady-state
228 ozone is derived from Eq. 4 of McLinden et al. (2000). The photochemical steady-state ozone
229 mole fraction f_{ss} (parts per million, moles per mole of dry air) is expressed as follows:

$$230 \quad f_{ss} = f_o + [(P - L)_o + \frac{\partial(P-L)}{\partial T}|_o (T - T_o) + \frac{\partial(P-L)}{\partial C_{O_3}}|_o (C_{O_3} - C_{O_3}^o)] \tau, \quad (2)$$

231 The values f_o , T_o , and $C_{O_3}^o$ are the climatological values of local ozone, temperature, and
232 overhead column ozone tables used to calculate the Linoz tendencies. $(P-L)_o$ is the ozone net
233 production minus loss tendency and the partial derivatives are the sensitivity of the net
234 production to temperature and overhead column ozone. All of these quantities are evaluated at
235 the climatological values and tabulated by Linoz as a function of month, pressure altitude, and
236 latitude. The effective lifetime of ozone, τ , is calculated from the Linoz tables as the negative
237 reciprocal of the tabulated partial derivative of the production with respect to ozone, i.e., $\tau =$
238 $-[\frac{\partial(P-L)}{\partial f}|_o]^{-1}$. A major assumption here is that the key chemical families (NOy, Cly, Bry)
239 and long-lived reactive gases (N₂O, CH₄, H₂O) do not change from their climatological values
240 used to generate the tables (Hsu and Prather, 2009). This steady-state calculation ignores
241 transport tendencies and thus will be apply only where the photochemistry is rapid, $\tau < 100$ days.



242 In application, we derive f_{ss} first locally from the T profile, and then calculate C_{O_3} to correct
243 for the column ozone sensitivity. Note the calculation of C_{O_3} includes the column ozone based
244 on the f_{ss} values from all the layers overhead plus a contribution from the local f_{ss} in that layer
245 weighted by the air mass in the upper half of the layer. Thus, equation 2 becomes a linear
246 algebraic equation involving f_{ss} . Fig. 2 shows this steady-state calculation (f_{ss} , T, τ) for January
247 and July using ERA5 monthly mean temperature.

248 **5. Impact of QBO on stratospheric ozone**

249 Nudging the tropical zonal wind creates QBO-driven perturbations to the temperature and
250 residual circulation that we can diagnose in both the E3SMv2 and CESM2 runs and compare
251 with observations. For E3SMv2 with interactive ozone we are able to see the changes in ozone.
252 This also applies to the simulations with an internally generated QBO.

253 We create a similar composite of the QBO cycle using E3SMv2/CESM2 following Ruiz et
254 al., (2021) to see the full QBO cycle influence on stratospheric ozone. The time-composite is
255 created for each month starting 14 months prior and extending to 14 months after the QBO
256 transition for 1979-2020. The center is when the NLPCA-derived QBO phase angle index (see
257 section 3) shifts from negative to positive (QBOe \rightarrow QBOw). We create the total column ozone
258 (TCO), tropical ozone, and extratropical ozone composite as a function of QBO phase. For the
259 TCO, we calculate the zonal-mean averages to produce the global map of composite. For tropical
260 (15°S - 15°N) and extratropical (30°S - 60°S / 30°N - 60°N) ozone, the data is processed to produce
261 vertical profiles of regional average ozone using latitudinal weight to produce the vertical profile
262 composite. The CESM2 ozone composite is not shown since its ozone is prescribed. To further
263 analyze the impact of QBO-induced circulation on ozone, the process is also repeated for
264 temperature, zonal wind and steady state ozone (see section 4). We first analyze the impact of
265 QBO on global TCO in section 5.1, and separately analyze impact on tropical and extratropical
266 stratospheric ozone in section 5.2 and 5.3, followed by the overall performance in section 5.4.

267 **5.1 Impact of QBO on global TCO**

268 In this section, we examine the impact of QBO on ozone using TCO observations (MSRv2)
269 and E3SMv2 model simulations. The TCO composites from E3SMv2 nudged and natural
270 simulations are compared in Fig. 3.



271 It is shown that the anomalous MSRV2 TCO exhibits a significant monopole-to-tripole
272 pattern from QBOe to QBOw (Fig. 3a). The TCO pattern exhibits a monopole pattern of
273 anomalous low during QBOe that gradually transits to tri-pole pattern of anomalous high in the
274 tropics and low in the extratropics. The magnitude of the negative in QBOe (5 DU) is lower than
275 the positive pattern (12 DU) in QBOw in the tropics, indicating asymmetric response of TCO to
276 QBO in the tropics. The E3SMv2 nudged simulation is like MSRV2 in that it captures most of
277 the monopole-to-tripole pattern within the tropics and extratropics with similar amplitudes (Fig.
278 3b), indicating the impact of nudged QBO on TCO is close to what observed. Internally
279 generated QBO variability in E3SMv2 natural, on the other hand, only partly exhibits the
280 patterns of MSRV2 (Fig. 3c) with weaker amplitude (nearly eight times weaker). This indicates
281 the QBO-related signal is partly present in natural E3SMv2, and that nudging the tropical zonal
282 wind contributes to the modulation and enhancement of this “QBO-driven” TCO variability.

283 **5.2 Impact of QBO on tropical stratospheric ozone**

284 In this section, we analyze the impact of QBO on tropical (15°S-15°N) stratospheric ozone
285 concentration. The composites of ozone vertical profile (1-hPa to 100-hPa) from E3SMv2
286 nudged and natural simulations are compared with the CMZM satellite data (Fig. 4).

287 It is shown that the CMZM satellite ozone exhibits a double-peak vertical structure with large
288 ozone variations between 1~20-hPa and 20~100-hPa (Fig. 4a). Both peaks shift in a sequence of
289 negative-positive-negative from QBOe to QBOw, and the amplitude of the upper peak is smaller
290 than that of the lower peak (Fig. 4a). The E3SMv2 nudged simulation captures parts of the
291 double-peak structure (Fig. 4b). The E3SMv2 natural simulations, on the other hand, show
292 similar double-peaked patterns but with smaller amplitude (3 times weaker) and shorter period
293 (Fig. 4c). This may be because the period of internally generated QBO in E3SMv2 is ~21 years
294 (Golaz et al., 2022). Overall, the E3SMv2 nudged simulation modifies the period and enhances
295 the QBO response in ozone that is mostly consistent with the CMZM weaker above 20-hPa and
296 stronger below 20-hPa.

297 As a coupled system, the QBO chemical and transport impacts on ozone are intertwined,
298 making it difficult to diagnose which QBO impact is more important to the ozone differences
299 between model and observation or among different models. Here we try to quantitatively
300 separate these two terms with a new diagnostic tool, recognizing their time scale differences. We
301 derive the steady state ozone (see Section 4 for details) for E3SM nudged and natural simulations



(Figs. 5a and 5c). The steady state ozone for CESM2 is also derived (Figs. 5b and 5d). Although ozone is prescribed in CESM2, the steady state ozone for CESM2 shown here is the “would-be” temperature-ozone if CESM2 were to implement Linoz v2 as its diagnostic ozone module. The steady state ozone in both E3SMv2 and CESM2 nudged simulations show similar patterns of ozone peak above 20-hPa while weak response below 20-hPa (Figs. 5a and 5b). The steady state ozone of E3SMv2 and CESM2 natural simulations (Figs. 5c and 5d) partly resemble that of the nudged simulations except with weaker amplitude and different periods (shorter for E3SMv2 and longer for CESM2). This corresponds to their similar alternating temperature pattern phase shift in the tropics (Figs. 6b, 6c, 6d and 6e) and indicates that the QBO impacts ozone through temperature-sensitive, fast chemical reactions above 20-hPa. The prognostic ozone in E3SMv2 below 20-hPa corresponds to the alternating \underline{w}^* shift patterns (Figs. 6g and 6i). This and the no response in steady state ozone indicates the prognostic ozone below 20-hPa in E3SMv2 is transport-driven. This demarcation of the QBO-induced ozone at 20-hPa may be due to the separation of ozone lifetime below/above 20-hPa (Reed et al., 1964). The ozone lifetime is relatively long compared with the dynamical process below this level while shortened considerably above it. The temperature affects ozone above 20-hPa through ozone destruction – colder/warmer anomalies slow/accelerate ozone destruction, leading to correspondent ozone increase/decrease (Wang et al., 2022); the transport effect of QBO-related wind modulates the temperature through thermal wind balance enhancing/lessening the upward motion in the tropics (Plumb and Bell, 1982; Baldwin et al., 2001; Ribera et al., 2004; Punge et al., 2009). This explains the apparent separation of transport- and chemistry-driven ozone changes above/below 20-hPa. It is also worth mentioning that the nudged CESM2 also produces similar temperature and \underline{w}^* (Figs. 6c and 6h), it thus indicates that nudged CESM2 may produce similar prognostic ozone if it were to implement Linoz v2 as interactive ozone module. Overall, there are apparent demarcation of QBO impact on tropical stratospheric ozone (15°S-15°N) above/below 20-hPa in the nudged runs that can separately be explained by transport and chemical impact.

5.3 Impact of QBO on extratropical stratospheric ozone

We extend the analysis of the impact of QBO on ozone to the extratropical region in both hemispheres (30°N-60°N/30°S-60°S). Since in the nudged simulations the nudging is imposed only in the tropical regions, we can further examine the impact of nudged QBO in the extratropics where it is free running. Fig. 7 shows pressure-time cross-section of the extratropical



(30°N-60°N/30°S-60°S) ozone concentration as a function of QBO phase for CMZM satellite ozone, E3SMv2 nudged, and E3SMv2 natural simulations. It is shown that nudged E3SMv2 simulations follow the similar positive-negative ozone phase shift in both hemispheres (Figs. 7b and 7e). The difference is that ozone is slightly stronger in QBOe while similar amplitude in QBOw. The natural E3SMv2 simulation does not reproduce the patterns of the nudged simulation for both hemispheres (Figs. 7c and 7f). This indicates that the nudged QBO is driving the phase shift of E3SMv2 ozone in both hemispheres' extratropic. For the natural simulations, the deficiency is likely due to the weak internally generated QBO in E3SMv2. Overall, the nudged E3SMv2 captures the QBO signal propagated outside of tropics and produces the extratropical ozone phase shift in both hemispheres. The natural simulation does not show the phase shift potentially due to weaker internally generated QBO.

In terms of the transport/chemical impact separation, we follow the analysis of Fig. 5 for E3SMv2 and CESM2 using the Linoz v2 model (Fig. 8). Like that of the analysis in the tropics, the chemical impact is stronger above 20-hPa for both E3SMv2 and CESM2 nudged simulations (Figs. 8a, 8b, 8e, and 8f), except the Southern Hemisphere (30°S-60°S) is overall noisier than that of the northern hemisphere (30°N-60°N). The natural simulations between the two models are different. The E3SMv2 natural simulations generally show consistent negative phase (Figs. 8c and 8g). The CESM2 natural simulations exhibits similar pattern to the nudged simulations in the northern hemisphere while that in the Southern Hemisphere is noisier (Figs. 8d and 8h). This noisier southern hemisphere steady state ozone above 20-hPa in the nudged simulations correspond to the noisier temperature for the two models (Figs. 9g and 9h), which may be largely affected by stronger and noisier southern polar vortex (Supplementary Figs. 5a and 5b) as also documented by other studies (Ribera et al., 2004). The intrusion of the polar vortex via events like stratospheric sudden warming (Butler et al., 2017) may have an impact on the QBO-ozone relationship in the extratropics. Below 20-hPa, the E3SMv2 nudged ozone corresponds to the \bar{w}^* (Fig. 9l and 9q), indicating it's transport-driven.

In terms of the impact of QBO nudging in the extratropics, there are considerable differences between the two models especially in the Southern Hemisphere. It shown that CESM2's phase shift of temperature and \bar{w}^* patterns (Figs. 9h and 9r) in the Southern Hemisphere is not as obvious as that shown in E3SM (Figs. 9g and 9q). Since this is outside the nudging region, it's complicated to differentiate the main impact factor. One reason may be the different ozone



364 feedback between the two models – interactive ozone in E3SMv2 contributes to maintain the
365 QBO-temperature structure (Butchart et al., 2023) while prescribed ozone in CESM2 does not;
366 Another may be due to the overall 3-D nudging strategy in E3SMv2 that may provide more
367 stringent constraint than the 2-D zonal mean nudging strategy that CESM2 adopted. Another
368 interesting issue is that both nudged simulations can partly reproduce the observed ERA5
369 temperature and \underline{w}^* patterns in the extratropic regions outside of the tropical nudging regions.
370 This occurrence of the residual circulation consistent with the ERA5 in the extratropics indicates
371 the validity of the nudging strategy for the QBOi protocol. Despite the fixed ozone, the CESM2
372 could still produce such circulation and temperature patterns that is consistent with ERA5
373 indicates the overall weak ozone feedback on formation of circulations both in the tropics and
374 extratropics. These patterns and the steady state ozone analysis for the CESM2 nudged
375 simulation also indicate that it may reproduce the prognostic ozone like E3SMv2 if it were to use
376 Linov2 as interactive ozone module under the QBOi nudging protocol.

377 **5.4 Model performance in simulating QBO impact**

378 In this sub-section, we examine the overall performance of E3SMv2 and CESM2 QBOi
379 simulations in simulating the QBO-ozone relationship. We evaluate the pattern correlation and
380 standard deviation of the area-weighted TCO pattern (60°S-60°N), vertically-weighted ozone
381 concentration (15°S-15°N, 30°N-60°N, 30°S-60°S), zonal wind (15°S-15°N, 30°N-60°N, 30°S-
382 60°S), temperature (15°S-15°N, 30°N-60°N, 30°S-60°S), and \underline{w}^* (15°S-15°N, 30°N-60°N, 30°S-
383 60°S). For ozone, only E3SMv2 results are shown since CESM2 has fixed ozone. The results are
384 summarized in a Taylor diagram shown in Fig. 10. The observed pattern is plotted at the (1,0)
385 reference point.

386 In terms of ozone (Fig. 10a), there are remarkable differences between the simulations.
387 Overall, the E3SMv2 nudged simulations perform the best, with the pattern correlation of all
388 four variables over 0.8 while other simulations are below 0.5. This indicates nudging realistic
389 QBO variability may increase the model performance in simulating ozone. In the extratropics,
390 the E3SMv2 nudged simulation has good pattern correlations, but the amplitude is off by over
391 1.5 times. The results for temperature, zonal wind and \underline{w}^* are similar with ozone in the tropics
392 (Figs. 10b, 10c, and 10d). What's different is in the extratropics — both nudged
393 E3SMv2/CESM2 temperature, zonal wind, and \underline{w}^* show better performance in NH extratropics



394 than in SH extratropics. This may be due to stronger polar vortices in SH and NH that disturb the
395 QBO signal. Another difference is in the natural simulations – the tropical temperature (15°S-
396 15°N) and zonal wind signals exhibit reasonable correlations of over 0.7 in zonal wind, over 0.5
397 in temperature. This indicates a discernable internally generated QBO signal in the
398 E3SMv2/CESM2, although it's weaker and does not extend to the extratropics.

399 **6. Discussion and Conclusion**

400 **6.1 Discussion**

401 There are some interesting issues worth mentioning in this study. The first is the effect of
402 nudging. It is shown that even in the extratropical regions where the QBO nudging is not
403 imposed, the QBO impact on extratropical circulation is still apparent in the two models. In these
404 QBOi simulations, the E3SMv2 employs a 3-D nudging strategy where the ERA5 3-D full field
405 zonal wind is nudged to the model while CESM2 employs a 2-D nudging strategy. It may be
406 recognized that the E3SMv2 posed a stronger nudging than CESM2, but both strategies were
407 able to produce extratropical QBO-associated circulation outside of the nudging region, this
408 demonstrates the overall effectiveness of the nudging strategy. Between the models, there are
409 still minor differences. For example, the extratropical zonal wind and temperature in CESM2 are
410 more scattered than that of E3SMv2. One reason may be the nudging strategy discussed above,
411 another reason may be the interactive/non-interactive ozone in the model. In this QBOi
412 simulation setup, E3SMv2 has the interactive ozone turned on, while CESM has only fixed
413 ozone input. Thus, the QBO-ozone interaction in E3SMv2 may be more self-consistent than that
414 in CESM2 – Studies have documented the impact of QBO-ozone interaction tend to maintain
415 and the QBO-temperature structure and prolong its period (Hasebe et al., 1994; Shibata, 2021;
416 Butchart et al., 2023).

417 Another noteworthy issue is the use of the offline Linoz v2 model to diagnose the dynamic
418 and chemical impact of QBO on ozone. It is demonstrated here that the Linoz v2 is a simple but
419 useful tool to diagnose and separate the dynamic/chemical impact of QBO on ozone. The results
420 shown here are important for diagnosing model-model and model-observation differences in the
421 QBO-ozone responses for climate simulations.

422 **6.2 Conclusion**



423 In this study, we utilize the Linoz v2 model to separate the chemical and transport response
424 of the QBO ozone impact in climate models. We derive a new QBO phase index using an
425 NLPCA method, and utilize the index to form QBO cycle composites to analyze QBO-ozone
426 relationship in observation and simulations produced under the QBOi protocol. By analyzing the
427 simulations of two QBOi participant models (E3SMv2 and CESM2), it is shown that the nudged
428 E3SMv2 simulation captures the monopole-to-tripole composite pattern in the observed TCO.
429 The natural simulation partly reproduces the observed TCO pattern but with weaker amplitude
430 and shorter period, indicating there is an internally generated QBO in E3SMv2 that is enhanced
431 and prolonged by nudging in the E3SMv2 nudged simulations. Looking further into the vertical
432 structure of the QBO-ozone relationship, it is shown that the E3SMv2 nudged simulations
433 capture most of the double-peaked vertical structure in observed ozone data between 1~20-hPa
434 and 20~100-hPa in the tropics but with weaker amplitudes in the extratropics. natural simulation
435 only captures part of the structure with smaller amplitude, indicating the existence of internally
436 generated QBO. This and the nudged simulations indicate that nudging enhanced the QBO
437 amplitude and prolonged its period originally exists within E3SMv2.

438 Utilizing the Linoz v2, we separated the chemical and transport response of ozone in
439 E3SMv2 nudged to QBO. It is shown that the two impacts have a rather clear demarcation on
440 both tropical and extratropical ozone response below/above 20-hPa – chemistry impact
441 correspondent to QBO-related temperature change dominates the response above 20-hPa linked
442 to photochemical process, and transport impact related to QBO-related vertical motion dominates
443 the response below 20-hPa. The results here are important for diagnosing model-model and
444 model-observation differences in the QBO with free-running climate-change simulations,
445 allowing us to separate temperature from circulation effects. In CESM2, the fixed ozone that is
446 out-of-phase with the observed QBO variability seems to impose a weak constraint on the overall
447 simulation. This indicates that using interactive ozone or not in the simulation does not
448 significantly alter the results for QBO simulations, although the synchronization impact of QBO
449 variability in observed ozone may need further examination (Butchart et al., 2023).

450 Stratospheric ozone is not only essential for protecting life on the Earth but also has
451 important climate impacts. More and more studies reported the important role of ozone
452 variations in modifying the stratospheric circulation and therefore influencing the surface climate
453 (e.g. Xie et al., 2020). Since the QBO has relatively high predictability, considering its impacts



on stratospheric ozone and subsequent atmospheric circulations may help improve the predictions of surface weather and climate (e.g., Li et al., 2023).

Despite the above studies, however, there are still caveats. Firstly, the current study makes use of only one model in QBOi that has interactive ozone feature. More models may be used in the future to examine the QBO-ozone relationship. The capability of the current version of O3v2 in E3SMv2 is limited due to the missing representation of the NO_x long-lived tracers. In the latest version of E3SMv3, the O3v2 is updated to include the impacts of these tracers, it would be interesting to see how these tracers interact with the current ozone calculations. These are to be assessed in future studies.

Data availability

The satellite data from the Copernicus Climate Change Service can be accessed at (<https://cds.climate.copernicus.eu/cdsapp#!/dataset/satellite-ozone-v1?tab=form>). The ERA5 data can be accessed at (<https://cds.climate.copernicus.eu/cdsapp#!/dataset/reanalysis-era5-complete?tab=overview>). The ChemDyg diagnostics can be accessed at (<https://doi.org/10.5281/zenodo.11166488>).

Author contribution

J.X., Q.T. designed the research; J.X. performed the E3SM simulations and wrote the manuscript. J.R. provided the CESM2 simulation. Q. T. and M.P.'s supervised the research and helped interpreting the results. All authors contributed to the scientific discussion and paper revision.

Competing interests

The authors declare that they have no conflict of interest.

Acknowledgement



483 We thank the Copernicus Climate Change Service for providing the satellite data and ECMWF
484 for the ERA5 data. We thank Isla Simpson for setting up the CESM2 QBOi simulations, and
485 providing the Python script for generating the Transformed Eulerian Mean variables. We thank
486 Sasha Glenville for transferring the CESM2 data. This research was supported as part of the
487 E3SM project, funded by the U.S. Department of Energy, Office of Science, Office of Biological
488 and Environmental Research. Part of the work was supported by the LLNL LDRD project 22-
489 ERD-008 titled “Multiscale Wildfire Simulation Framework and Remote Sensing”. E3SM
490 simulations were performed on a high-performance computing cluster provided by the BER
491 ESM program and operated by the Laboratory Computing Resource Center at Argonne National
492 Laboratory. Additional post-processing and data archiving of production simulations used
493 resources of the National Energy Research Scientific Computing Center (NERSC), a DOE
494 Office of Science User Facility supported by the Office of Science of the U.S. Department of
495 Energy under Contract No. DE-AC02-05CH11231. This work was performed under the auspices
496 of the U.S. Department of Energy by Lawrence Livermore National Laboratory under contract
497 DE-AC52-07NA27344. The IM release number is LLNL-JRNL-858987. This work was in part
498 supported by the National Center for Atmospheric Research (NCAR), which is a major facility
499 sponsored by the National Science Foundation (NSF) under Cooperative Agreement 1852977.
500 Portions of this study were supported by the Regional and Global Model Analysis (RGMA)
501 component of the Earth and Environmental System Modeling Program of the U.S. Department of
502 Energy’s Office of Biological and Environmental Research (BER) via NSF Interagency
503 Agreement 1844590.



504 Reference

- 505 Andrews, M. B., Knight, J. R., Scaife, A. A., et al.: Observed and Simulated Teleconnections
506 Between the Stratospheric Quasi-Biennial Oscillation and Northern Hemisphere Winter
507 Atmospheric Circulation, *J. Geophys. Res.*, 124, 1219–1232,
508 <https://doi.org/10.1029/2018JD029368>, 2019.
- 509 Andrews, D.G., J.R. Holton, and C.B. Leovy: *Middle Atmosphere Dynamics*. Academic Press,
510 489pp, 1987.
- 511 Anstey, J. A. and Shepherd, T. G.: High-latitude influence of the quasi-biennial oscillation, *Q.*
512 *J. Roy. Meteor. Soc.*, 140, 1–21, <https://doi.org/10.1002/qj.2132>, 2014.
- 513 Baldwin, M. P., Birner, T., Brasseur, G., et al.: 100 years of progress in understanding the
514 stratosphere and mesosphere, *Meteor. Mon.*, 59, 27.1–27.62,
515 <https://doi.org/10.1175/AMSMONOGRAPHSD-19-0003.1>, 2019.
- 516 Baldwin, M. P., Gray, L. J., Dunkerton, T. J., et al., The quasi-biennial oscillation, *Rev.*
517 *Geophys.*, 39, 179–229, 2001.
- 518 Baldwin M. P., Tung K.K., Extra-tropical QBO signals in angular momentum and wave forcing.
519 *Geophys. Res. Lett.* 21: 2717–2720, 1994.
- 520 Beljaars, A. C. M., Brown, A. R., & Wood, N.: A new parameterization of turbulent orographic
521 form drag. *Quarterly Journal of the Royal Meteorological Society*, 130, 1327–1347.
522 <https://doi.org/10.1256/qj.03.73>, 2004.
- 523 Bowman, K. P.: Global patterns of the quasi-biennial oscillation in total ozone. *J. Atmos.*
524 *Sci.*, 46, 3382–3343, 1989.
- 525 Brasseur, G., Hauglustaine, D., Walters, S., Rasch, P., Muller, J., Granier, C., & Tie, X:
526 MOZART, a global chemical transport model for ozone and related chemical tracers 1. Model
527 description. *Journal of Geophysical Research-Atmospheres*, 103(D21), 28,265–28,289.
528 <https://doi.org/10.1029/98JD02397>, 1998.
- 529 Burkholder, J. B., Sander, S. P., Abbatt, J., Barker, J. R., Huie, R. E., Kolb, C. E., et al.:
530 Chemical kinetics and photochemical data for use in atmospheric studies, evaluation no. 18,
531 JPL Publication 15–10, Jet Propulsion Laboratory, Pasadena, CA. Retrieved from
532 <http://jpldataeval.jpl.nasa.gov>, 2015.
- 533 Bushell, A. C., Anstey, J. A., Butchart, N., et al.: Evaluation of the quasi-biennial oscillation in
534 global climate models for the SPARC QBO-initiative. *Quarterly Journal of the Royal*
535 *Meteorological Society*, 148(744), 1459–1489, 2020.
- 536 Butchart, N., Andrews, M. B., & Jones, C. D.: QBO phase synchronization in CMIP6 historical
537 simulations attributed to ozone forcing. *Geophysical Research Letters*, 50, e2023GL104401.
538 <https://doi.org/10.1029/2023GL104401>, 2023.
- 539 Butchart, N., Anstey, J. A., Hamilton, K., et al.: Overview of experiment design and
540 comparison of models participating in phase 1 of the SPARC Quasi-Biennial Oscillation
541 initiative (QBOi). *Geoscientific Model Development*, 11(3), 1009–1032, 2018.
- 542 Butchart, N., Charlton-Perez, A. J., Cionni, I., et al.: Multimodel climate and variability of the
543 stratosphere, *J. Geophys. Res.*, 116, D05102, <https://doi.org/10.1029/2010JD014995>, 2011.
- 544 Butchart, N., Scaife, A.A., Austin, J., et al.: Quasi-biennial oscillation in ozone in a coupled
545 chemistry-climate model. *J. Geophys. Res.: Atmosphere* 108 (D15), 4486, 2003.
- 546 Butler, A. H., Sjöberg, J. P., Seidel, D. J., Rosenlof, K. H.: A sudden stratospheric warming
547 compendium, *Earth System Science Data*. 9 (1): 63–76. doi:10.5194/essd-9-63-2017.



- 548 Charron, M., and Manzini, E.: Gravity waves from fronts: Parameterization and middle
549 atmosphere response in a general circulation model. *Journal of the Atmospheric Sciences*,
550 59(5), 923– 941. [https://doi.org/10.1175/1520-0469\(2002\)059<0923:gwffpa>2.0.co;2](https://doi.org/10.1175/1520-0469(2002)059<0923:gwffpa>2.0.co;2), 2002.
- 551 Chipperfield, M. P., & Gray, L. J. : Two-dimensional model studies of the interannual
552 variability of trace gases in the middle atmosphere. *Journal of Geophysical Research:*
553 *Atmospheres*, 97(D5), 5963-5980, 1992.
- 554 Chipperfield, M. P., Gray, L. J., Kinnersley, J. S., Zawodny, J.: A two-dimensional model study
555 of the QBO signal in SAGE II NO₂ and O₃. *Geophysical research letters*, 21(7), 589-592,
556 1994.
- 557 Coy, L., Wargan, K., Molod, A. M., et al.: Structure and dynamics of the quasi-biennial
558 oscillation in MERRA-2, *J. Climate*, 29, 5339–5354, 2016.
- 559 Danabasoglu, G., Lamarque, J.-F., Bacmeister, J. et al.: The Community Earth System Model
560 Version 2 (CESM2). *Journal of Advances in Modeling Earth Systems*, 12, e2019MS001916.
561 <https://doi.org/10.1029/2019MS001916>, 2020.
- 562 Dunkerton, T. J.: The role of gravity waves in the quasi-biennial oscillation, *J. Geophys. Res.*,
563 102, 26,053-26,076, 1997.
- 564 Elsbury, D., Peings, Y., and Magnusdottir, G.: Variation in the Holton-Tan effect by longitude,
565 *Q. J. Roy. Meteor. Soc.*, 147, 1767–1787, <https://doi.org/10.1002/qj.3993>, 2021.
- 566 Emmons, L. K., Schwantes, R. H., Orlando, J. J., et al.: The Chemistry Mechanism in the
567 Community Earth System Model version 2 (CESM2). *Journal of Advances in Modeling Earth*
568 *Systems*, 12, e2019MS001882. <https://doi.org/10.1029/2019MS001882>, 2020.
- 569 Emmons, L. K., Hauglustaine, D. A., Müller, J. F., Carroll, M. A., Brasseur, G. P., Brunner, D.,
570 et al.: Data composites of airborne observations of tropospheric ozone and its precursors.
571 *Journal of Geophysical Research-Atmospheres*, 105(D16), 20497–20538.
572 <https://doi.org/10.1029/2000jd900232>, 2000.
- 573 Garfinkel, C. I., Shaw, T. A., Hartmann, D. L., and Waugh, D.W.: Does the Holton-Tan
574 Mechanism Explain How the Quasi-Biennial Oscillation Modulates the Arctic Polar Vortex?, *J.*
575 *Atmos. Sci.*, 69, 1713–1733, <https://doi.org/10.1175/JAS-D-11-0209.1>, 2012.
- 576 Gettelman, A., & Morrison, H.: Advanced two-moment bulk microphysics for global models.
577 Part I: Off-line tests and comparison with other schemes. *Journal of Climate*, 28, 1268–1287.
578 <https://doi.org/10.1175/JCLI-D-14-00102.1>, 2015.
- 579 Giorgetta, M. A., Manzini, E., and Roeckner, E.: Forcing of the quasi-biennial oscillation from
580 a broad spectrum of atmospheric waves. *Geophysical Research Letters*, 29(8), 86-1, 2002.
- 581 Golaz, J.-C., Van Roekel, L. P., Zheng, X. et al. : The DOE E3SM Model version 2: Overview
582 of the physical model and initial model evaluation. *Journal of Advances in Modeling Earth*
583 *Systems*, 14, e2022MS003156. <https://doi.org/10.1029/2022MS003156>, 2022.
- 584 Golaz, J.-C., Caldwell, P. M., Van Roekel, L. P. et al.: The DOE E3SM coupled model version
585 1: Overview and evaluation at standard resolution. *Journal of Advances in Modeling Earth*
586 *Systems*, 11(7), 2089– 2129. <https://doi.org/10.1029/2018MS001603>, 2019.
- 587 Golaz, J.-C., Larson, V. E., & Cotton, W. R. A PDF-based model for boundary layer clouds.
588 Part I: Method and model description. *Journal of the Atmospheric Sciences*, 59, 3540–3551,
589 2002.
- 590 Gray, L. J., & Dunkerton, T. J.: The role of the seasonal cycle in the quasi-biennial oscillation
591 of ozone. *Journal of Atmospheric Sciences*, 47(20), 2429-2452, 1990.



- 592 Hamilton, K., & Hsieh, W. W.: Representation of the quasi-biennial oscillation in the tropical
593 stratospheric wind by nonlinear principal component analysis. *Journal of Geophysical*
594 *Research: Atmospheres*, 107(D15), ACL-3, 2002.
- 595 Hamilton, K. : Interhemispheric asymmetry and annual synchronization of the ozone quasi-
596 biennial oscillation. *Journal of Atmospheric Sciences*, 46(7), 1019-1025, 1989.
- 597 Hansen, F., Matthes, K., and Gray, L. J.: Sensitivity of stratospheric dynamics and chemistry to
598 QBO nudging width in the chemistryclimate model WACCM, *J. Geophys. Res.*, 118, 10464–
599 10474, <https://doi.org/10.1002/jgrd.50812>, 2013.
- 600 Hasebe, F.: Quasi-biennial oscillations of ozone and diabatic circulation in the equatorial
601 stratosphere, *J. Atmos. Sci.*, 51, 729–745, 1994.
- 602 Hersbach H, Bell B, Berrisford P, et al.: The ERA5 global reanalysis, *Q J R Meteorol Soc.*
603 2020; 146: 1999–2049. <https://doi.org/10.1002/qj.3803>, 2020,
- 604 Hitchcock, P., Butler, A., Charlton-Perez, A., et al.: Stratospheric Nudging And Predictable
605 Surface Impacts (SNAPSI): a protocol for investigating the role of stratospheric polar vortex
606 disturbances in subseasonal to seasonal forecasts. *Geoscientific Model Development*, 15(13),
607 5073-5092, 2022.
- 608 Hitchman, M. H., and C. B. Leovy: Estimation of the Kelvin wave contribution to the
609 semiannual oscillation, *J. Atmos. Sci.*, 45, 1462, 1988.
- 610 Holton, J. R. and Tan, H.-C.: The quasi-biennial oscillation in the Northern Hemisphere lower
611 stratosphere, *J. Meteor. Soc. Japan.*, 60, 140–148, 1982.
- 612 Holton, J. R. and Tan, H.-C.: The influence of the equatorial quasi-biennial oscillation on the
613 global circulation at 50 mb, *J. Atmos. Sci.*, 37, 2200–2208, 1980.
- 614 Holton, J. R.: Influence of the annual cycle in meridional transport on the quasi-biennial
615 oscillation in total ozone. *Journal of Atmospheric Sciences*, 46(10), 1434-1439, 1989.
- 616 Holton, J. R., and R. S. Lindzen: An updated theory for the quasi-biennial cycle of the tropical
617 stratosphere, *J Atmos. Sci.*, 29, 1076, 1972.
- 618 Horowitz, L. W., Walters, S., Mauzerall, D. L., Emmons, L. K., Rasch, P. J., Granier, C., et al.:
619 A global simulation of tropospheric ozone and related tracers: Description and evaluation of
620 MOZART, version 2. *Journal of Geophysical Research-Atmospheres*, 108(D24), 4784.
621 <https://doi.org/10.1029/2002jd002853>, 2003.
- 622 Hsu, J. and Prather, M. J.: Stratospheric variability and tropospheric ozone, *J. Geophys. Res.-*
623 *Atmos.*, 114, D06102, <https://doi.org/10.1029/2008JD010942>, 2009.
- 624 Hsu, J., M. J. Prather, and O. Wild: Diagnosing the stratosphere-totroposphere flux of ozone in
625 a chemistry transport model, *J. Geophys. Res.*, 110, D19305, doi:10.1029/2005JD006045, 2005.
- 626 Isla et al.: Toward the vertical resolution of the next generation of the Community Atmosphere
627 Model, To be submitted, 2024.
- 628 Jones, D. B., Schneider, H. R., & McElroy, M. B.: Effects of the quasi-biennial oscillation on
629 the zonally averaged transport of tracers. *Journal of Geophysical Research: Atmospheres*,
630 103(D10), 11235-11249, 1998.
- 631 Jucker, M., Reichler, T., & Waugh, D. W.: How frequent are Antarctic sudden stratospheric
632 warmings in present and future climate?. *Geophysical Research Letters*, 48(11),
633 e2021GL093215, 2021.
- 634 Kang, M. J., Chun, H. Y., Son, S. W., et al.: Role of tropical lower stratosphere winds in quasi-
635 biennial oscillation disruptions. *Science Advances*, 8(27), eabm7229, 2022.
- 636 Kinnersley, J. S., and Tung, K. K.: Mechanisms for the extratropical QBO in circulation and
637 ozone. *Journal of the atmospheric sciences*, 56(12), 1942-1962, 1999.



- 638 Kinnison, D. E., Brasseur, G. P., Walters, S., Garcia, R. R., Marsh, D. R., Sassi, F., et al.:
639 Sensitivity of chemical tracers to meteorological parameters in the MOZART-3 chemical
640 transport model. *Journal of Geophysical Research-Atmospheres*, 112(D20), D20302.
641 <https://doi.org/10.1029/2006jd007879>, 2007.
- 642 Lamarque, J. F., Emmons, L. K., Hess, P. G., Kinnison, D. E., Tilmes, S., Vitt, F., et al.: CAM-
643 chem: Description and evaluation of interactive atmospheric chemistry in the Community Earth
644 System Model. *Geoscientific Model Development*, 5(2), 369–411. <https://doi.org/10.5194/gmd-5-369-2012>, 2012.
- 645
646 Larson, V. E. : CLUBB-SILHS: A parameterization of subgrid variability in the atmosphere.
647 arXiv:1711.03675v2 [physics.ao-ph], 2017.
- 648 Lawrence, B. N. : A gravity-wave induced quasi-biennial oscillation in a three-dimensional
649 mechanistic model. *Quarterly Journal of the Royal Meteorological Society*, 127(576), 2005-
650 2021, 2001.
- 651 Lee, S., Shelow, D., Thompson, A.M., Miller, S.: QBO and ENSO variability in temperature
652 and ozone from SHADOZ, 1998–2005. *J. Geophys. Res.: Atmosphere* 115 (D18105), 2010.
- 653 Lee, H.-H., Tang, Q., and Prather, M.: E3SM Chemistry Diagnostics Package (ChemDyg)
654 Version 0.1.4, *Geosci. Model Dev. Discuss.* [preprint], <https://doi.org/10.5194/gmd-2023-203>,
655 in review, 2024.
- 656 Leung, L. R., Bader, D. C., Taylor, M. A., and McCoy, R. B.: An introduction to the E3SM
657 special collection: Goals, science drivers, development, and analysis. *Journal of Advances in*
658 *Modeling Earth Systems*, 12, e2019MS001821, 2020. <https://doi.org/10.1029/2019MS001821>
- 659 Li, Y., Richter, J. H., Chen, C.-C., & Tang, Q.: A strengthened teleconnection of the quasi-
660 biennial oscillation and tropical easterly jet in the past decades in E3SMv1. *Geophysical*
661 *Research Letters*, 50, e2023GL104517. <https://doi.org/10.1029/2023GL104517>, 2023.
- 662 Lin, S. J., & Rood, R. B.: An explicit Flux-Form Semi-Lagrangian shallow water model on the
663 sphere. *Quarterly Journal of the Royal Meteorological Society*, 123, 2477–2498.
- 664 Lindzen, R. S., and J. R. Holton (1968), A theory of the quasi-biennial oscillation, *J. Atmos.*
665 *Sci.*, 25, 1095, 1997.
- 666 Logan, J. A., M. J. Prather, S. C. Wofsy, and M. B. McElroy: Atmospheric Chemistry -
667 Response to Human Influence. *Philos T R Soc A*, 290, 187-234, 1978.
- 668 Lu, B. W., Pandolfo, L., and Hamilton, K.: Nonlinear representation of the quasi-biennial
669 oscillation. *Journal of the atmospheric sciences*, 66(7), 1886-1904, 2009.
- 670 Marquardt, C., & Naujokat, B.: An update of the equatorial QBO and its variability. *World*
671 *Meteorological Organization-Publications-WMO TD*, 1, 87-90, 1997.
- 672 Maycock, A. C., Randel, W. J., Steiner, A. K., Karpechko, A. Y., Christy, J., Saunders, R., et
673 al.: Revisiting the mystery of recent stratospheric temperature trends, 2018. *Geophysical*
674 *Research Letters*, 45, 9919–9933. <https://doi.org/10.1029/2018GL078035>
- 675 McFarlane, N. A.: The effect of orographically excited gravity wave drag on the general
676 circulation of the lower stratosphere and troposphere. *Journal of the Atmospheric Sciences*,
677 44(14), 1775–1800. [https://doi.org/10.1175/1520-0469\(1987\)044<1775:teooeg>2.0.co;2](https://doi.org/10.1175/1520-0469(1987)044<1775:teooeg>2.0.co;2),
678 1987.
- 679 McLinden, C. A., Olsen, S. C., Hannegan, B., et al.: Stratospheric ozone in 3-D models: A
680 simple chemistry and the cross-tropopause flux, *J. Geophys. Res.*, 105(D11), 14653–14665,
681 doi:10.1029/2000JD900124, 2000.
- 682 Mengel, J. G., H. G. Mayr, K. L. Chan, et al.: Equatorial oscillations in the middle atmosphere
683 generated by small-scale gravity waves, *Geophys. Res. Lett.*, 22, 3027-3030, 1995.



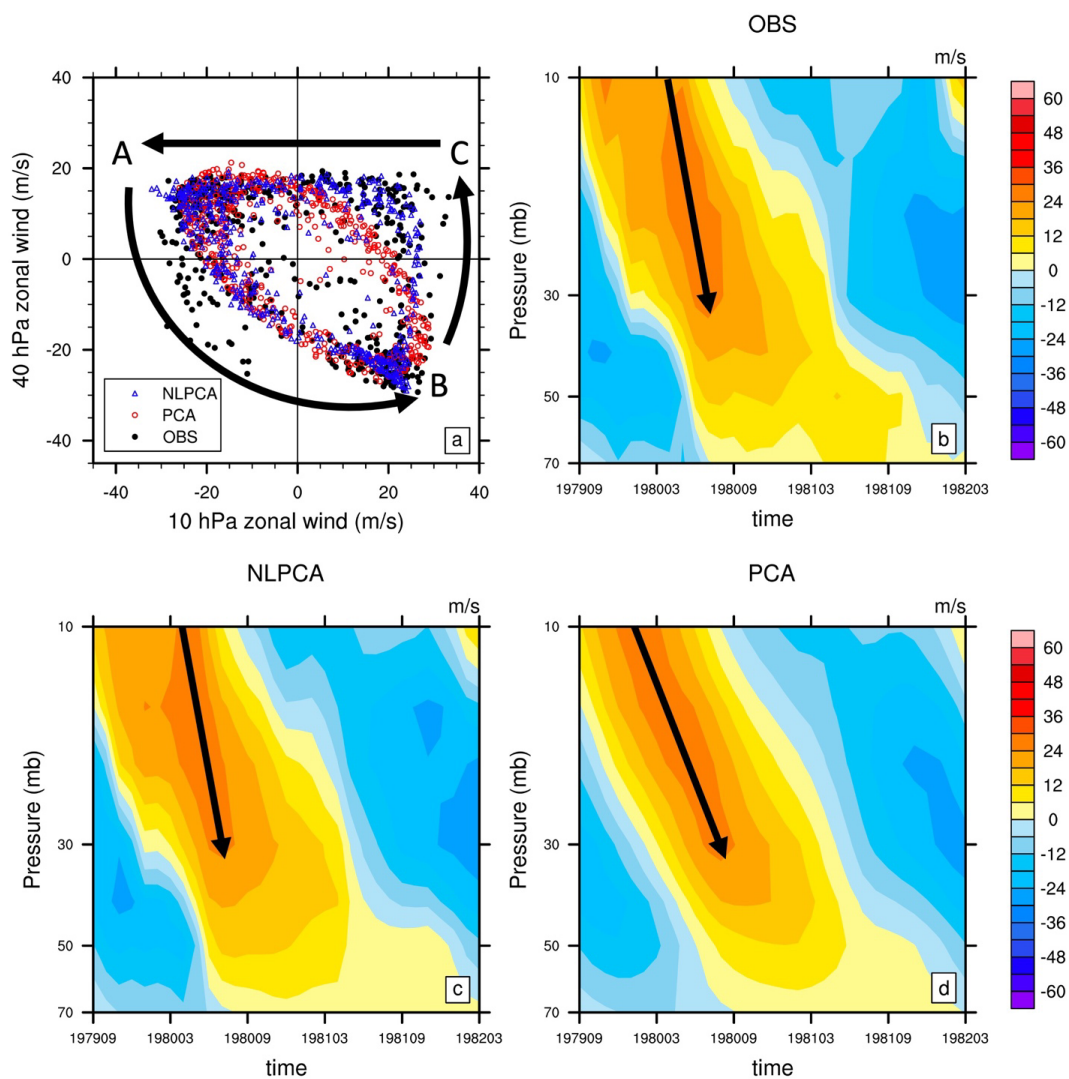
- 684 Morgenstern, O., Hegglin, M. I., Rozanov, E., et al.: Review of the global models used within
685 phase 1 of the Chemistry–Climate Model Initiative (CCMI), *Geosci. Model Dev.*, 10, 639–671,
686 <https://doi.org/10.5194/gmd-10-639-2017>, 2017.
- 687 Naujokat, B.: An update of the observed quasi-biennial oscillation of the stratospheric winds
688 over the tropics. *J. Atmos. Sci.*, 43, 1873–1877, 1986.
- 689 Orbe, C., Plummer, D. A., Waugh, D. W., et al.: Description and Evaluation of the specified-
690 dynamics experiment in the Chemistry–Climate Model Initiative, *Atmos. Chem. Phys.*, 20,
691 3809–3840, <https://doi.org/10.5194/acp-20-3809-2020>, 2020.
- 692 Park, M., and Coauthors: Variability of stratospheric reactive nitrogen and ozone related to the
693 QBO. *J. Geophys. Res. Atmos.*, 122, 10 103–10 118, <https://doi.org/10.1002/2017JD027061>,
694 2017.
- 695 Pahlavan, H. A., Fu, Q., Wallace, J. M., & Kiladis, G. N.: Revisiting the quasi-biennial
696 oscillation as seen in ERA5. Part I: Description and momentum budget. *Journal of the*
697 *Atmospheric Sciences*, 78(3), 673–691, 2021a.
- 698 Pahlavan, H. A., Wallace, J. M., Fu, Q., & Kiladis, G. N.: Revisiting the quasi-biennial
699 oscillation as seen in ERA5. Part II: Evaluation of waves and wave forcing. *Journal of the*
700 *Atmospheric Sciences*, 78(3), 693–707, 2021b.
- 701 Park, M., Randel, W. J., Kinnison, D. E., et al.: Variability of stratospheric reactive nitrogen
702 and ozone related to the QBO. *Journal of Geophysical Research: Atmospheres*, 122(18), 10-
703 103, 2017.
- 704 Pawson, S., K. Labitzke, R. Lenschow, et al.: Climatology of the Northern Hemisphere
705 stratosphere derived from Berlin analyses, art 1, Monthly means, technical report, Ser.A ,7(3),
706 Freie Univ. Berlin, 1993.
- 707 PhotoComp: Chapter 6 - Stratospheric Chemistry SPARC Report No. 5 on the Evaluation of
708 Chemistry–Climate Models 194–202, 2010.
- 709 Plumb, R. A., and R. C. Bell: A model of the quasi-biennial oscillation on an equatorial beta-
710 plane, *Q. J. R. Meteorol. Soc.*, 108, 335–352, 1982.
- 711 Prather, J. M., Remsberg, E. E.: The Atmospheric Effects of Stratospheric Aircraft: Report of
712 the 1992 Models and Measurements Workshop. (M.J. Prather, E.E. Remsberg, Eds.), Satellite
713 Beach, FL, 144+268+352 pp, 1993.
- 714 Politowicz, P. A., & Hitchman, M. H.: Exploring the effects of forcing quasi-biennial
715 oscillations in a two-dimensional model. *Journal of Geophysical Research: Atmospheres*,
716 102(D14), 16481–16497, 1997.
- 717 Randall, D. A., Tziperman, E., Branson, M. D., Richter, J. H., & Kang, W. :The QBO-MJO
718 connection: A possible role for the SST and ENSO. *Journal of Climate*, 1–36, 2023.
- 719 Randel, W. J., & Cobb, J. B.: Coherent variations of monthly mean total ozone and lower
720 stratospheric temperature. *Journal of Geophysical Research: Atmospheres*, 99(D3), 5433–5447,
721 1994.
- 722 Randel, W. J., Wu, F., Russell, J. M., Roche, A., & Waters, J. W.: Seasonal cycles and QBO
723 variations in stratospheric CH₄ and H₂O observed in UARS HALOE data. *Journal of the*
724 *atmospheric sciences*, 55(2), 163–185, 1998.
- 725 Randel, W. J., and F. Wu: Isolation of the ozone QBO in SAGE II data by singular value
726 decomposition. *J. Atmos. Sci.*, **53**, 2546–2559, 1996.
- 727 Rasch, P. J., Xie, S., Ma, P.-L., et al.: An overview of the atmospheric component of the
728 Energy Exascale Earth System Model. *Journal of Advances in Modeling Earth Systems*, 11(8),
729 2377– 2411. <https://doi.org/10.1029/2019ms001629>, 2019.



- 730 Reed, R.: A tentative model of the 26-month oscillation in tropical latitudes. *Q. J. R. Meteorol.*
731 *Soc.* 90, 441–466, 1964.
- 732 Richter, J. H., Anstey, J. A., Butchart, N., Kawatani, Y., Meehl, G. A., Osprey, S., & Simpson,
733 I. R.: Progress in simulating the quasi-biennial oscillation in CMIP models. *Journal*
734 *Geophysical Research: Atmospheres*, 125, e2019JD032362.
735 <https://doi.org/10.1029/2019JD032362>, 2020.
- 736 Richter, J. H., Chen, C.-C., Tang, Q., et al.: Improved simulation of the QBO in E3SMv1.
737 *Journal of Advances in Modeling Earth Systems*, 11(11), 3403– 3418.
738 <https://doi.org/10.1029/2019MS001763>, 2019.
- 739 Ruiz, D. J., Prather, M. J., Strahan, S. E., et al.: How atmospheric chemistry and transport drive
740 surface variability of N₂O and CFC-11. *Journal of Geophysical Research: Atmospheres*, 126,
741 e2020JD033979. <https://doi.org/10.1029/2020JD033979>, (2021).
- 742 Ruiz, D. J. and M.J. Prather: From the middle stratosphere to the surface, using nitrous oxide to
743 constrain the stratosphere–troposphere exchange of ozone, *Atmos. Chem. Phys.*, 22, 2079–
744 2093, doi: 10.5194/acp-22-2079-2022, 2022.
- 745 Sander, et al. : Chemical kinetics and photochemical data for use in atmospheric studies,
746 evaluation number 15, in JPL Publication 06-2., Jet Propul. Lab., Pasadena, Calif., 2006.
- 747 Scholz M. and Vigário R.: Nonlinear PCA: a new hierarchical approach, *Proceedings of the*
748 *10th European Symposium on Artificial Neural Networks (ESANN)*, pp. 439-444., 2002.
- 749 Schwartz, M., Froidevaux, L., Livesey, N., Read, W., and Fuller, R.: MLS/Aura Level 3
750 Monthly Binned Ozone (O₃) Mixing Ratio on Assorted Grids V005, Greenbelt, MD, USA,
751 Goddard Earth Sciences Data and Information Services Center (GES DISC) [data set],
752 https://disc.gsfc.nasa.gov/datasets/ML3MBO3_005/summary (last access: 30 May 2024), 2021.
- 753 Scinocca, J., & Mcfarlane, N.: The parametrization of drag induced by stratified flow over
754 anisotropic orography. *Quarterly Journal of the Royal Meteorological Society*, 126, 2353–2394.
755 <https://doi.org/10.1256/smsqj.56801>, 2000.
- 756 Shibata, K.: Simulations of Ozone Feedback Effects on the Equatorial Quasi-Biennial
757 Oscillation with a Chemistry–Climate Model. *Climate*, (9), 123.
758 <https://doi.org/10.3390/cli9080123>, 2021.
- 759 Shuckburgh, E., Norton, W., Iwi, A., & Haynes, P.: Influence of the quasi-biennial oscillation
760 on isentropic transport and mixing in the tropics and subtropics. *Journal of Geophysical*
761 *Research: Atmospheres*, 106(D13), 14327–14337, 2001.
- 762 Sofieva, V. F., Szelag, M., Tamminen, J., et al.: Updated merged SAGE-CCI-OMPS+ dataset
763 for the evaluation of ozone trends in the stratosphere, *Atmos. Meas. Tech.*, 16, 1881–1899,
764 <https://doi.org/10.5194/amt-16-1881-2023>, 2023.
- 765 Tang, Q., Prather, M. J., Hsu, et al.: Evaluation of the interactive stratospheric ozone (O₃v2)
766 module in the E3SM version 1 Earth system model, *Geosci. Model Dev.*, 14, 1219–1236,
767 <https://doi.org/10.5194/gmd-14-1219-2021>, 2021.
- 768 Tang, Q., Golaz, J.-C., Van Roekel, L. P.: The fully coupled regionally refined model of E3SM
769 version 2: overview of the atmosphere, land, and river results, *Geosci. Model Dev.*, 16, 3953–
770 3995, <https://doi.org/10.5194/gmd-16-3953-2023>, 2023.
- 771 Tang, Q., P. G. Hess, B. Brown-Steiner, and D. E. Kinnison : Tropospheric ozone decrease due
772 to the Mount Pinatubo eruption: Reduced stratospheric influx, *Geophys. Res. Lett.*, 40, 5553–
773 5558, doi: [10.1002/2013GL056563](https://doi.org/10.1002/2013GL056563), 2013.



- 774 Tian, W., Chipperfield, M.P., Gray, L.J., Zawodny, J.M.: Quasi-biennial oscillation and tracer
775 distributions in a coupled chemistry-climate model. *J. Geophys. Res.: Atmosphere* 111 (D20),
776 2006.
- 777 Tilmes, S., Lamarque, J. F., Emmons, L. K., Kinnison, D. E., Ma, P. L., Liu, X., et al.:
778 Description and evaluation of tropospheric chemistry and aerosols in the Community Earth
779 System Model (CESM1.2). *Geoscientific Model Development*, 8(5), 1395–1426.
780 <https://doi.org/10.5194/gmd-8-1395-2015>, 2015.
- 781 Tilmes, S., Lamarque, J. F., Emmons, L. K., Kinnison, D. E., Marsh, D., Garcia, R. R., et al.:
782 Representation of the Community Earth System Model (CESM1) CAM4-chem within the
783 Chemistry-Climate Model Initiative (CCMI). *Geoscientific Model Development*, 9(5), 1853–
784 1890. <https://doi.org/10.5194/gmd-9-1853-2016>, 2016.
- 785 Tung, K. K., and H. Yang: Global QBO in circulation and ozone. Part I: Reexamination of
786 observational evidence. *J. Atmos. Sci.*, **51**, 2699–2707, 1994.
- 787 Tweedy, O. V., Kramarova, N. A., Strahan, S. E., et al., (2017), Response of trace gases to the
788 disrupted 2015–2016 quasi-biennial oscillation, *Atmos. Chem. Phys.*, 17, 6813–6823, 2017.
- 789 van der A, R. J., Allaart, M. A. F., and Eskes, H. J.: Extended and refined multi sensor
790 reanalysis of total ozone for the period 1970–2012, *Atmos. Meas. Tech.*, 8, 3021–3035,
791 <https://doi.org/10.5194/amt-8-3021-2015>, 2015.
- 792 Wallace, J., Panetta, R., and Estberg, J.: Representation of the equatorial stratospheric
793 quasibiennial oscillation in EOF phase space, *J. Atmos. Sci.*, 50, 1751–1762,
794 [https://doi.org/10.1175/1520-0469\(1993\)050<1751:ROTESQ>2.0.CO;2](https://doi.org/10.1175/1520-0469(1993)050<1751:ROTESQ>2.0.CO;2), 1993.
- 795 Wang L., Hardiman, S. C., Bett, P. E. et al.: What chance of a sudden stratospheric warming in
796 the southern hemisphere?. *Environmental Research Letters*, 15 (10): 104038.
797 doi:10.1088/1748-9326/aba8c1. ISSN 1748-9326, 2020.
- 798 Wang, W., Hong, J., Shangguan, M., et al.: Zonally asymmetric influences of the quasi-biennial
799 oscillation on stratospheric ozone. *Atmospheric Chemistry and Physics*, 22(20), 13695–13711,
800 2022.
- 801 Watson, P. A. G. and Gray, L. J.: How Does the Quasi-Biennial Oscillation Affect the
802 Stratospheric Polar Vortex?, *J. Atmos. Sci.*, 71, 391–409, [https://doi.org/10.1175/JAS-D-13-](https://doi.org/10.1175/JAS-D-13-096.1)
803 096.1, 2014.
- 804 Xie, F., Zhang, J., Li, X., et al.: Independent and joint influences of eastern Pacific El Niño–
805 southern oscillation and quasi biennial oscillation on Northern Hemispheric stratospheric
806 ozone, *Int. J. Climatol.*, 12, 5289–5307, <https://doi.org/10.1002/joc.6519>, 2020.
- 807 Xie, S., Lin, W., Rasch, P. J., et al.: Understanding cloud and convective characteristics in
808 version 1 of the E3SM Atmosphere Model. *Journal of Advances in Modeling Earth Systems*,
809 10(10), 2618–2644. <https://doi.org/10.1029/2018ms001350>, 2018.
- 810 Zhang, J., Xie, F., Ma, Z., et al.: Seasonal Evolution of the Quasibiennial Oscillation Impact on
811 the Northern Hemisphere Polar Vortex in Winter, *J. Geophys. Res.*, 124, 12568–12586,
812 <https://doi.org/10.1029/2019JD030966>, 2019.
- 813 Zhang, J., Xie, F., Ma, Z., Zhang, C., et al.: Seasonal Evolution of the Quasibiennial Oscillation
814 Impact on the Northern Hemisphere Polar Vortex in Winter, *J. Geophys. Res.*, 124, 12568–
815 12586, <https://doi.org/10.1029/2019JD030966>, 2019.
- 816 Zhang, R., Tian, W., and Wang, T.: Role of the quasi-biennial oscillation in the downward
817 extension of stratospheric northern annular mode anomalies, *Clim. Dynam.*, 55, 595–612, 2019.
- 818



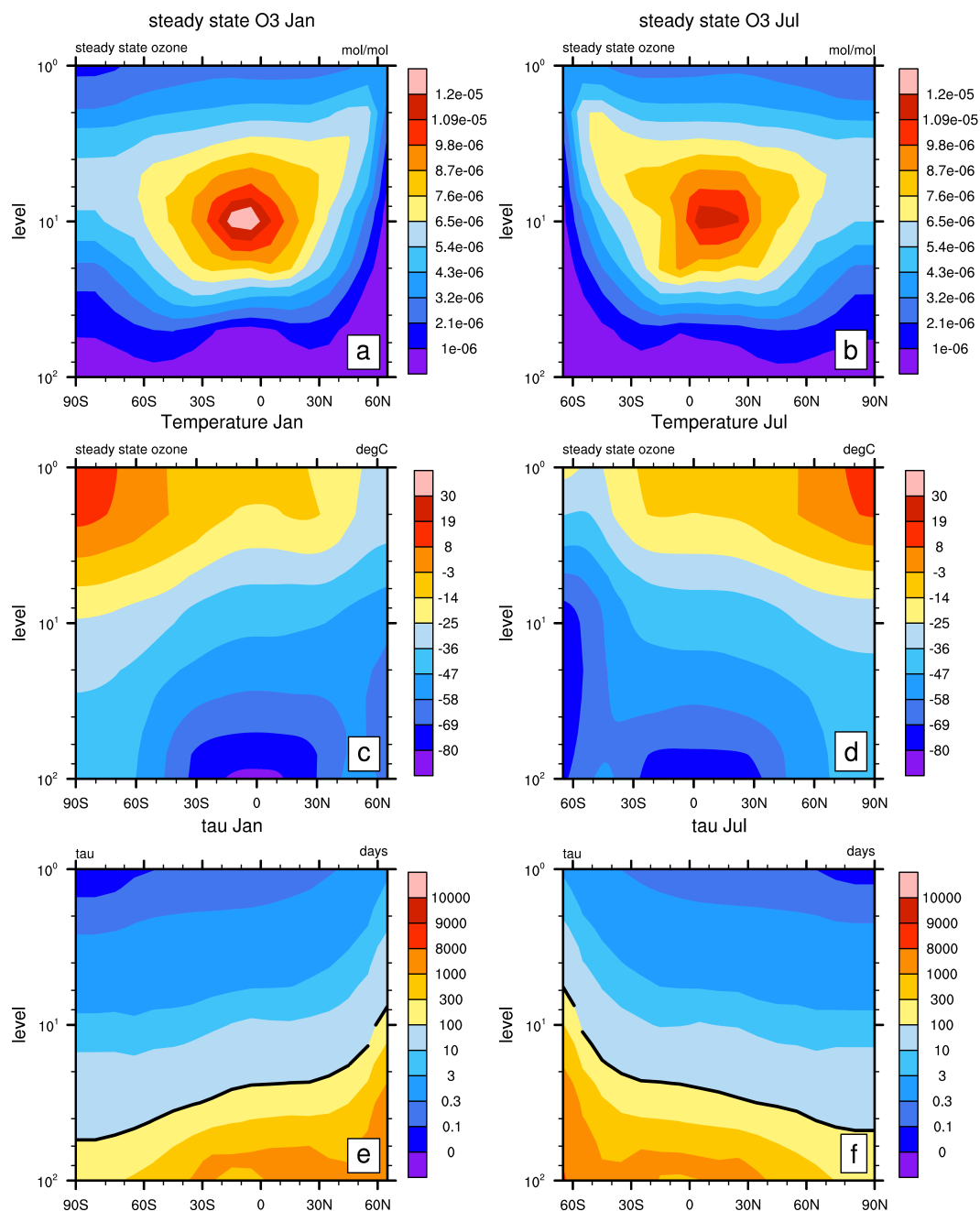
819

820 Fig. 1 (a) Scatter-plot of 1979-2020 anomalous monthly mean zonal wind (m/s) at 10-hPa vs 40-
821 hPa for observation (black), NLPCA reconstruction (blue), and PCA reconstruction (red).

822 Typical cycle of QBO from (b) Observational station data from University of Berlin, (c) NLPCA
823 reconstruction, (d) PCA reconstruction.

824

825





827 Fig. 2 The (a, b) steady state ozone (mol/mol) derived using LINOZ on E3SMv2 temperature, (c,
828 d) ERA5 temperature ($^{\circ}\text{C}$), (e, f) photochemical relaxation time τ (days), and for January and
829 July. The thick black line in (c, d) denotes the 300 value-line.
830

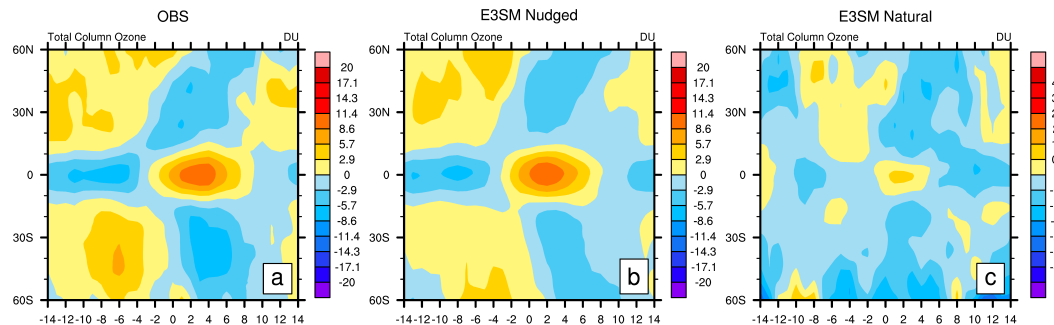
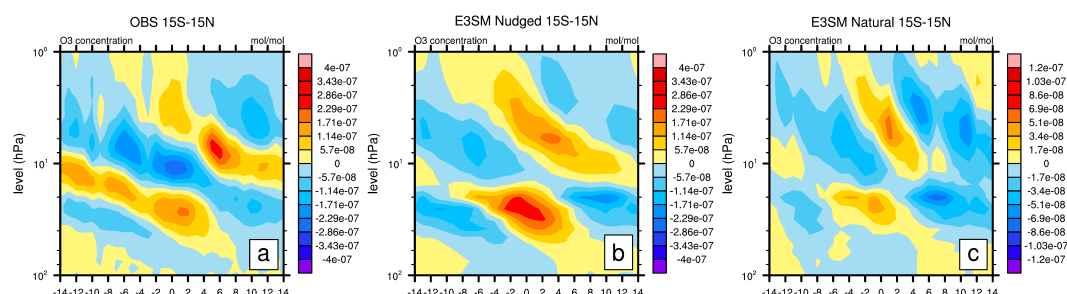


Fig. 3 Total column ozone (TCO, Dobson Unit) anomaly (relative to 1979-2020 mean) composites as function of QBO phase (determined by NLPCA QBO index) for (a) OBS (Multi-Sensor Reanalysis version 2), (b) E3SMv2 nudged simulation, (c) E3SMv2 natural simulation. 0 is centered on the month when QBO transits from QBOe to QBOw (determined by when current QBO index<0 and next QBO index>0). The QBO phase is determined by 5S-5N average of the zonal wind.

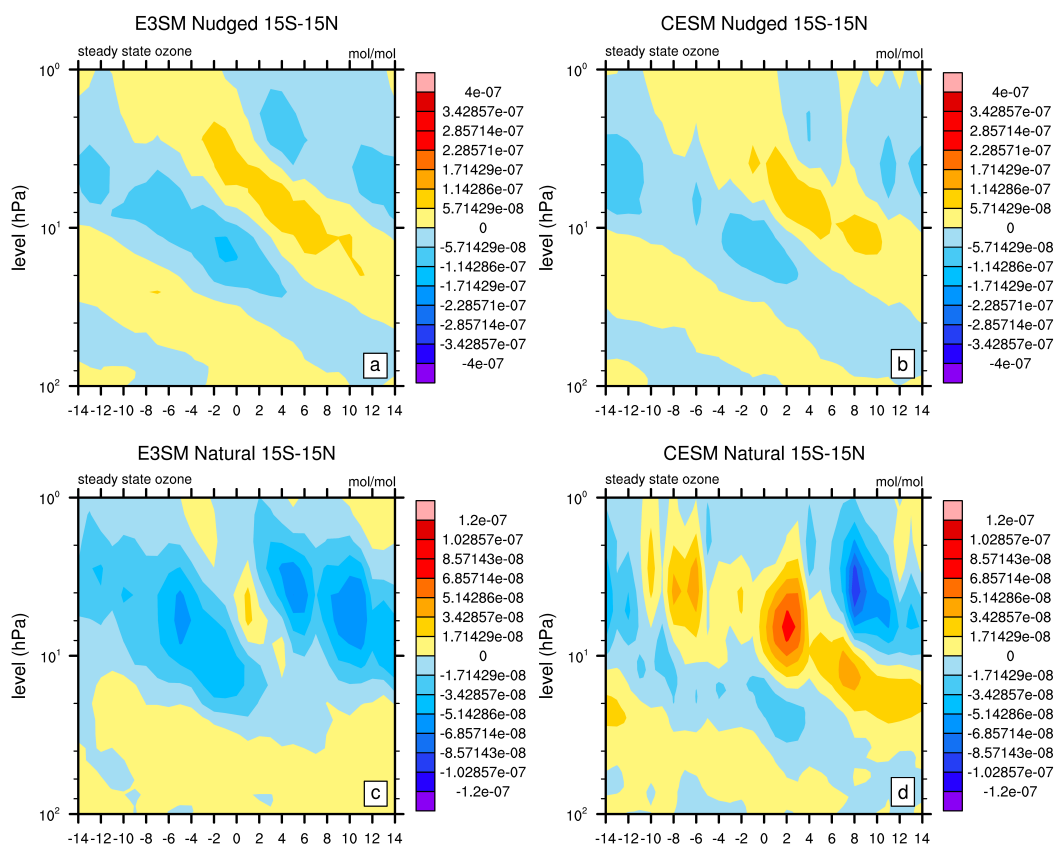


840

841 Fig. 4 Pressure-time cross-section of the tropical (15°S-15°N) 1979-2020 anomalous ozone
842 concentration (mol/mol) as function of QBO phase for (a) OBS (Concentration Monthly Zonal
843 Mean), (b) E3SMv2 nudged simulation, (c) E3SMv2 natural simulation. 0 is centered on the
844 month when QBO transits from QBOe to QBOw (determined by when current QBO index<0
845 and next QBO index>0). The QBO phase is determined by 5S-5N average of the zonal wind.

846

847



848

849

850

851

852

853

854

Fig. 5 Pressure-time cross-section of the tropical (15°S-15°N) 1979-2020 anomalous Linz steady state ozone (mol/mol) as function of QBO phase for (a, c) E3SMv2 and (c, d) CESM2. 0 is centered on the month when QBO transits from QBOe to QBOw (determined by when current QBO index<0 and next QBO index>0). The QBO phase is determined by 5S-5N average of the zonal wind.

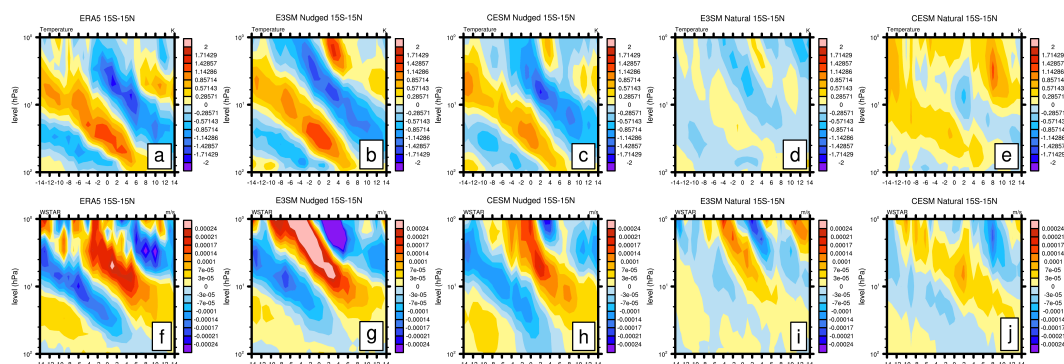
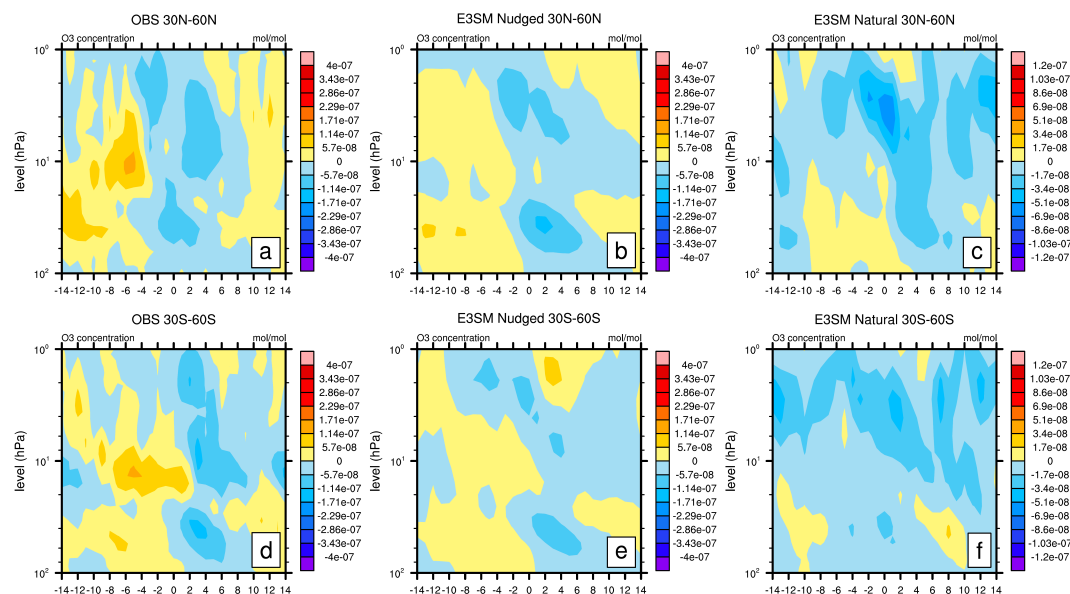


Fig. 6 Pressure-time cross-section of the tropical (15°S-15°N) 1979-2020 anomalous temperature (K) and \bar{w}^* (Transformed Eulerian Mean residual vertical transport, m/s) as function of QBO phase for (a, f) ERA5, (b, d, g, i) E3SMv2, (c, e, QBOe, j) CESM2. 0 is centered on the month when QBO transits from QBOe to QBOw (determined by when current QBO index < 0 and next QBO index > 0). The QBO phase is determined by 5S-5N average of the zonal wind.



863

864 Fig. 7 Pressure-time cross-section of the extratropical (30°N-60°N/30°S-60°S) 1979-2020
 865 anomalous ozone concentration (mol/mol) as function of QBO phase for (a, d) OBS (CMZM),
 866 (b, e) E3SMv2, (c, f) CESM2. 0 is centered on the month when QBO transits from QBOe to
 867 QBOw (determined by when current QBO index<0 and next QBO index>0). The QBO phase is
 868 determined by 5S-5N average of the zonal wind.

869

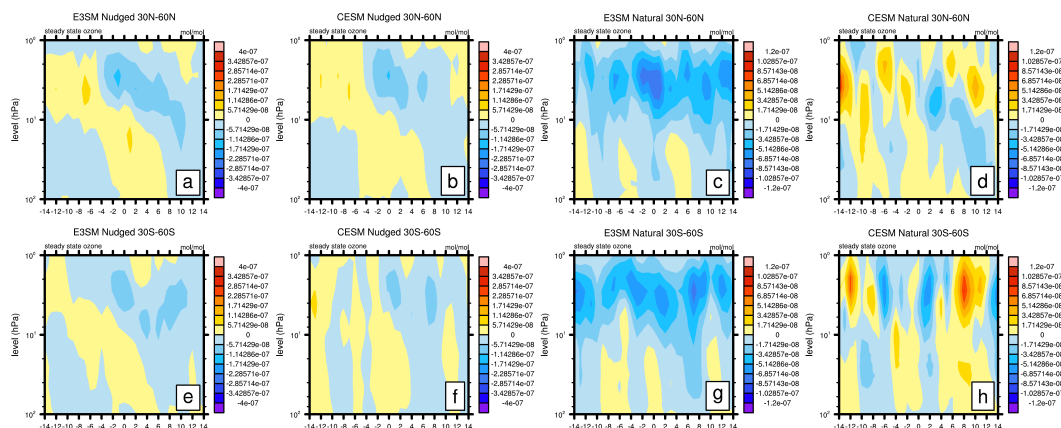
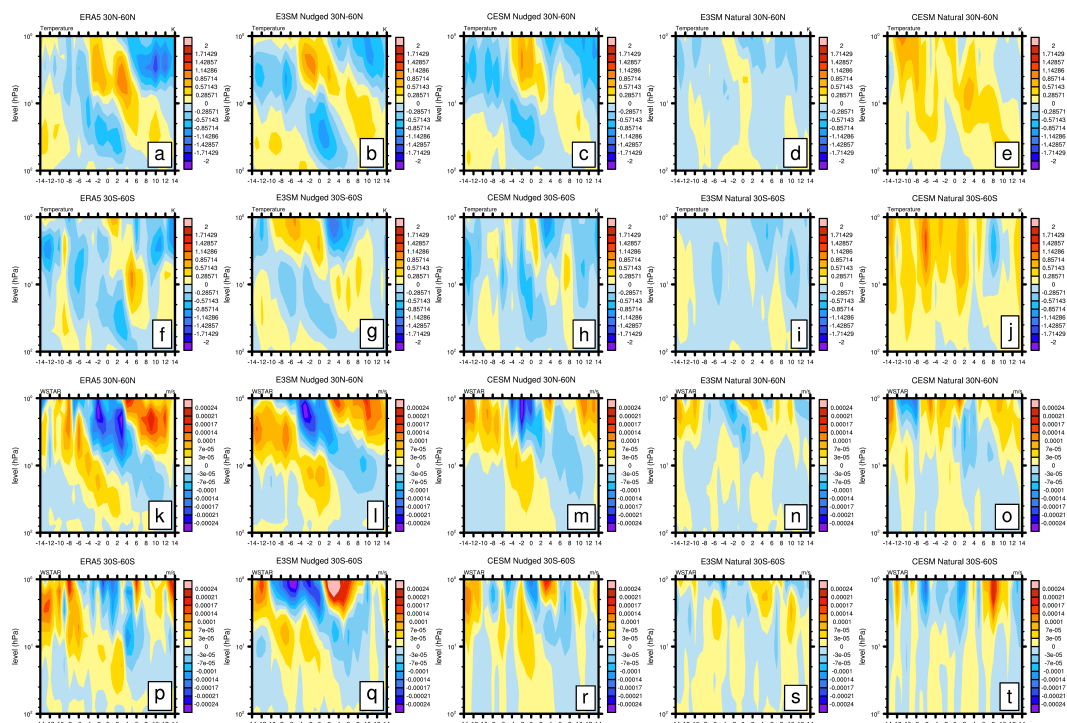


Fig. 8 Pressure-time cross-section of the extratropical (30°N-60°N/30°S-60°S) 1979-2020 anomalous steady state ozone (mol/mol) as function of QBO for (a, e) E3SMv2 nudged, (b, f) CESM2 nudged, (c, g) E3SMv2 natural, (d, h) CESM2 natural. 0 is centered on the month when QBO transits from QBOe to QBOw (determined by when current QBO index < 0 and next QBO index > 0). The QBO phase is determined by 5S-5N average of the zonal wind.

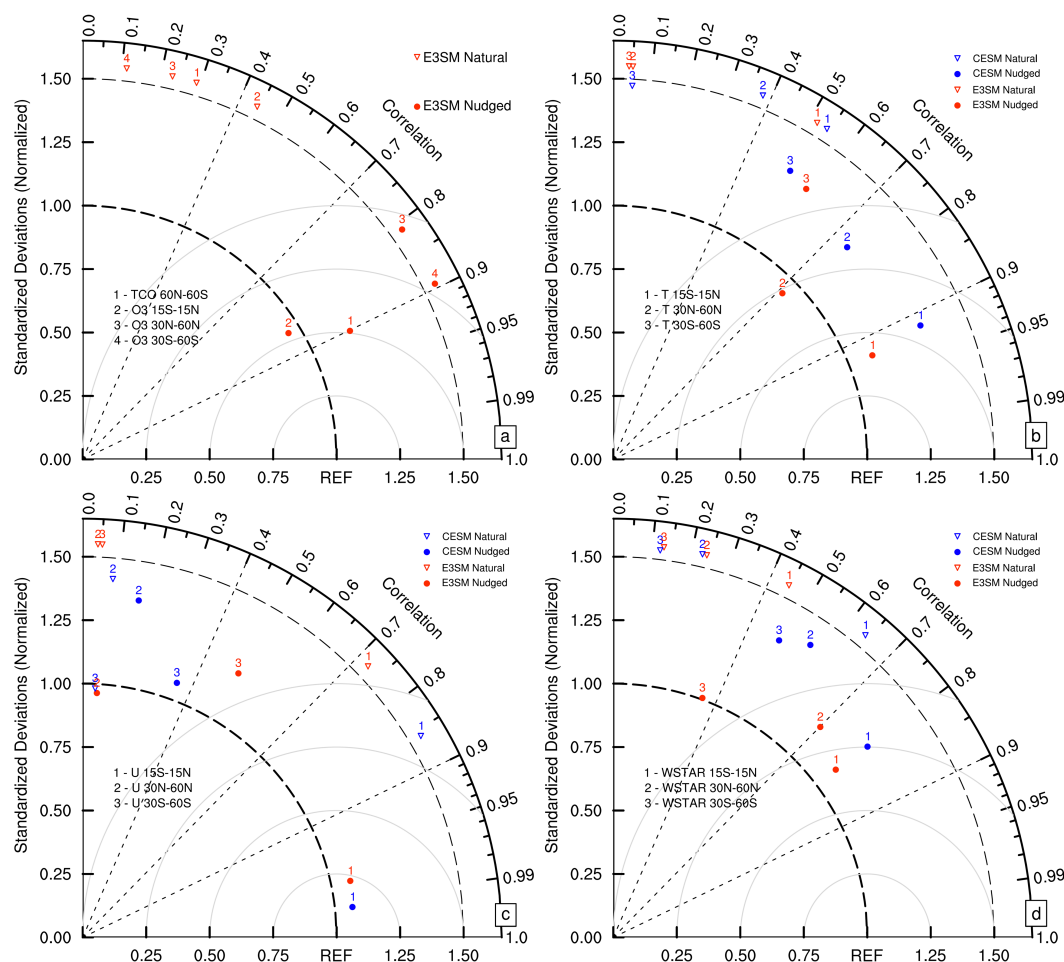


881



882

883 Fig. 9 Pressure-time cross-section of the extratropical (30°N-60°N/30°S-60°S) 1979-2020
884 temperature (K)/ \bar{u}^* (m/s) as function of QBO for (a, f, k, p) ERA5, (b, g, l, q) E3SMv2 nudged,
885 (c, QBOe, m, r) CESM2 nudged, (d, i, n, s) E3SMv2 natural, (e, j, o, t) CESM2 natural. CESM2.
886 0 is centered on the month when QBO transits from QBOe to QBOw (determined by when
887 current QBO index < 0 and next QBO index > 0). The QBO phase is determined by 5S-5N average
888 of the zonal wind.



889

890 Fig. 10 Taylor diagram of the E3SMv2/CESM2 simulation for various datasets for 1979-2020.

891 (a) The area-weighted total column ozone (60°S-60°N, DU) and pressure-time cross-sections of
 892 ozone concentration (15°S-15°N, 30°N-60°N, 30°S-60°S, mol/mol) anomalies with OBS (MSR
 893 and CMZM), respectively. (b) The area-weighted pressure-time cross-sections of temperature
 894 (15°S-15°N, 30°N-60°N, 30°S-60°S, K) anomalies with ERA5. (c) The area-weighted pressure-
 895 time cross-sections of zonal wind (15°S-15°N, 30°N-60°N, 30°S-60°S, m/s) anomalies with
 896 ERA5. For pattern correlations, the cross-sections are weighted by pressure layer thickness. On
 897 all Taylor diagrams, the model standard deviations are normalized by dividing the standard
 898 deviations of the reference.

899

<https://doi.org/10.5194/egusphere-2024-1927>

Preprint. Discussion started: 3 July 2024

© Author(s) 2024. CC BY 4.0 License.



900

901

902

903